Available online at www.sciencedirect.com

ScienceDirect

Procedia Structural Integrity 39 (2022) 347–363

Structural Integrity Procedia

www.elsevier.com/locate/procedia

7th International Conference on Crack Paths

Fatigue crack propagation studies based on the plastic component of the CTOD evaluated from Digital Image Correlation data

Muhammad Ajmal[1], Cristina Lopez-Crespo[1,2], Alejandro. S. Cruces[1], Fernando V. Antunes[3], Pablo Lopez-Crespo[1*]

1 Department of Civil and Materials Engineering, University of Malaga, C/ Doctor Ortiz Ramos, s/n, 29071 Malaga, Spain – plopezcrespo@uma.es

2 Politechnic Institute Jesus Marin, C/Politecnico, 1, 29007 Malaga, Spain

3 CEEMPRE, Department of Mechanical Engineering, University of Coimbra, Portugal

Abstract

This work presents a new approach based on the Crack Tip Opening Displacement (CTOD) for studying the fatigue crack growth. The plastic component of the CTOD is employed for predicting the crack propagation on austenitic stainless steel. This is in contrast to Linear Elastic Fracture Mechanics analysis based on the Stress Intensity Factor (SIF) (Ewalds and Wanhill 1984). The current method is also valid beyond Small Scale Yielding (Antunes et al. 2016)(Antunes et al. 2017a)(Borges et al. 2020) as it incorporates naturally the plasticity effects taking place at the crack tip (Lopez-Crespo et al. 2018). The approach is based on post-processing the full-field displacement information generated by Digital Image Correlation technique (Chernyatin et al. 2018). Such technique is used to monitor the crack advance throughout the test (Cruces et al. 2020). The post-processing procedure employed for extracting the plastic component of the CTOD is described in detail. The results on steel CT specimens appear very promising.

Keywords: Plastic component of CTOD; Austenitic stainless steel; Fatigue crack growth

* Corresponding author. Tel.: +0-000-000-0000 ; fax: +0-000-000-0000 .
E-mail address: bluedot66@gmail.com

10.1016/j.prostr.2022.03.104

1. Introduction

The damage tolerance approach for the designing of components assumes the presence of intrinsic defects due to manufacturing processes like casting, machining, welding, and additive manufacturing. These small defects grow into larger cracks during operation mainly due to fatigue. Fracture toughness of a material measures its resistance against crack growth, helps a designer to decide that how long a component can be in service with the presence of pre-existing cracks. The knowledge of fatigue crack growth rates (FCGR) become very important to estimate the time between inspections during crack monitoring.

Nomenclature

a	crack length
CJP	Christopher-James-Patterson (model)
CT	compact tension (specimen)
CTOD	crack tip opening displacement
$CTOD_e$	elastic CTOD
$CTOD_p$	plastic CTOD
da/dN	fatigue crack growth rate
DIC	digital image correlation
FCGR	fatigue crack growth rate
F_{cl}	crack closure load
$F_{ep,L}$	load corresponding to elastic-plastic transition
F_{max}	maximum applied load
F_{min}	minimum applied load
F_{op}	crack opening load
F_U	force applied during unloading
K_{max}	maximum stress intensity factor
ΔK	stress intensity factor range
ΔK_{eff}	effective stress intensity factor
$\Delta CTOD_p$	plastic CTOD range
LEFM	Linear Elastic Fracture Mechanics
$S_{e,L}$	slope of elastic regime during loading
$S_{e,U}$	slope of elastic regime during unloading
W	specimen width
U_{op}	crack opening level
U_{cl}	crack closure level

Many models have been proposed in the literature to quantify the fatigue crack growth rates (FCGR) depending up the loading conditions and material parameters. The most simple and well known model to predict FCGR rate da/dN is a power law described by Paris and Erdogan (Paris and Erdogan 1963) using stress intensity factor (SIF) range (ΔK) as

$$\frac{da}{dN} = C\left(\Delta K\right)^m \tag{1}$$

where C and m are constants dependent on the materials and the environmental factors.

The above relation has been extensively used due to the availability of analytical solutions for standard specimen and structural components submitted to cyclic loading. The use of SIF in fatigue studies is based on the assumption that crack tip damage is controlled by the surrounding elastic field (Rice 1967) and for long cracks having small-scale

yielding retains the advantage of Linear Elastic Fracture Mechanics (LEFM) (Paris and Erdogan 1963). The use of SIF is also helpful to quantify the effect of crack size and loading conditions on stress singularity.

However, there are some limitations in the use of stress intensity factor range as a driving force for FCGR: i) Inability to explain load ratio and variable amplitude effects, and its inconsistent behavior observed for short cracks(Antunes et al. 2019) and ii) da/dN-ΔK relations do not add understanding as a driving mechanism for fatigue crack growth because the units of both parameters are totally different. Therefore, to overcome these limitations different concepts have been introduced. Elber (Elber 1971) introduced the concept of crack closure assuming that the part of load cycle during which the crack flanks are in contact does not contribute to fatigue crack growth and modified the Paris Law by replacing ΔK with ΔK_{eff} as follows:

$$\frac{da}{dN} = C\left(\Delta K_{eff}\right)^{m} \tag{2}$$

Where ΔK is the SIF range (between the opening load and maximum load)

This concept has been applied successfully to address the effects of load ratio, load history, short cracks and stress state, but the quantification of crack closure levels are dependent on measurement procedures, along with according to several authors its irrelevance under plain strain conditions (Vasudevan, Sadananda, and Louat 1992).

Similarly, several other solutions were proposed like the concept of partial crack closure (Donald and Paris 1999)(Kujawski 2001b), the use of K_{max} along with ΔK (Kujawski 2001a)(Noroozi, Glinka, and Lambert 2005), T-stress (Lugo and Daniewicz 2011)(Larsson and Carlsson 1973) (Miarka et al. 2020a)(Miarka et al. 2020b) to consider the effect of specimen geometry and CJP model (Christopher et al. 2007) proposing four parameters to describe the stresses around the crack-tip. However, ΔK has limited application to describe fatigue crack growth, being an elastic parameter while crack growth is believed to be controlled by non-linear and irreversible parameters occurring at the crack-tip. Consequently, many researchers focused themselves to study FCG based on stress and strain fields (Noroozi, Glinka, and Lambert 2005), energy dissipated at crack-tip (Zheng et al. 2013), and cyclic J-Integral (Ktari et al. 2014). Crack-tip plastic deformation can be better described by two parameters naming J-Integral and crack tip opening displacement (CTOD). It is believed that CTOD serves better being a local parameter.

The concept of da/dN-$\Delta CTOD_p$ (plastic component range of CTOD) was originally presented by Antunes et al. (Antunes et al. 2016)(Antunes et al. 2017b)(Antunes et al. 2018) making use of numerical data for the extraction of $\Delta CTOD_p$. The main objective of the present work is to obtain a da/dN-$\Delta CTOD_p$ model for austenitic stainless steel from full-field displacement data collected by using Digital Image Correlation (DIC).

2. Experimental Details

2.1. Materials and specimen

The material used in the study is 316L austenitic stainless-steel alloy having a Young's modulus, E around 195 GPa and yield stress, σ_0 = 304 MPa. Fatigue crack growth specimens were prepared following a standard CT specimen configuration according to (ASTM E647−13 2014). The specimen to be considered as thick is specified according to the ratio of the thickness, B to the uncracked ligament length, $(W-a)$, as $B/(W-a) \geq 1$. Due to experimental limitations, the ratio of the thickness to the uncracked ligament length was chosen to be 0.5 for thick CT (B = 12 mm) specimen.

2.2. Fatigue crack growth experiments

Four specimens were used in this experimental study. For reference purposes the critical fracture toughness of these thin specimens was determined to be $Kc = 35MPa\sqrt{m}$ (Yusof, Lopez-Crespo, and Withers 2013). The experiments were conducted at room temperature for fatigue crack growth on a servo-hydraulic testing machine with a ±10 kN loading range. A schematic diagram of the experiment is shown in Fig. 1. The specimen was fatigued at a frequency,

f = 30 Hz and the DIC images were captured at various stages of crack growth at a much lower fatigue frequency (1/100 Hz). The loading amplitude was represented by maximum and minimum loads of P_{max} = 2.95 kN and P_{min} = 0.15 kN.

The DIC method described by (Yusof and Withers 2009)(Lopez-Crespo et al. 2013) was applied in this work. The experimental setup comprised a macro-lens with a tele-convertor mounted on a 4-mega pixel CCD camera (see Fig. 1). The light source was a fiber-optic ring attached to the periphery of the lens to achieve uniform illumination of the specimen surface. The surface had been abraded with silicone carbide medium grit paper to obtain a random texture giving sufficient contrast for the correlation algorithm.

2.3. Crack monitoring by digital image correlation

An area of 10 mm × 10 mm was imaged corresponding to 2048 × 2048 pixels from which each pixel represents about 5 μm. DIC was performed using LaVision image correlation software (GmbH 1999).

3. Measurement of CTOD

CTOD is a parameter that measures the opening at the crack tip. After performing the correlation between the images, a post processing routine has been used to identify the change of crack tip opening displacement, ΔCTOD, at various distances behind the crack-tip (Yusof, Lopez-Crespo, and Withers 2013) by subtracting the vertical displacements (u_y direction shown in Fig. 2) of the top flank and bottom flank across the crack:

$$\Delta CTOD(x) = u_y^{top} - u_y^{bot} \tag{3}$$

The x and y directions are shown in Fig.1 &2. CTOD is dependent on the distance behind the crack-tip along x direction keeping other parameters same. The vertical displacement of top and bottom flanks before and after loading at some selected distance behind the crack-tip is observed by DIC technique. The above equation holds good to find ΔCTOD i) in case of the setup as shown in Fig.1 or ii) the load is applied through wedge.

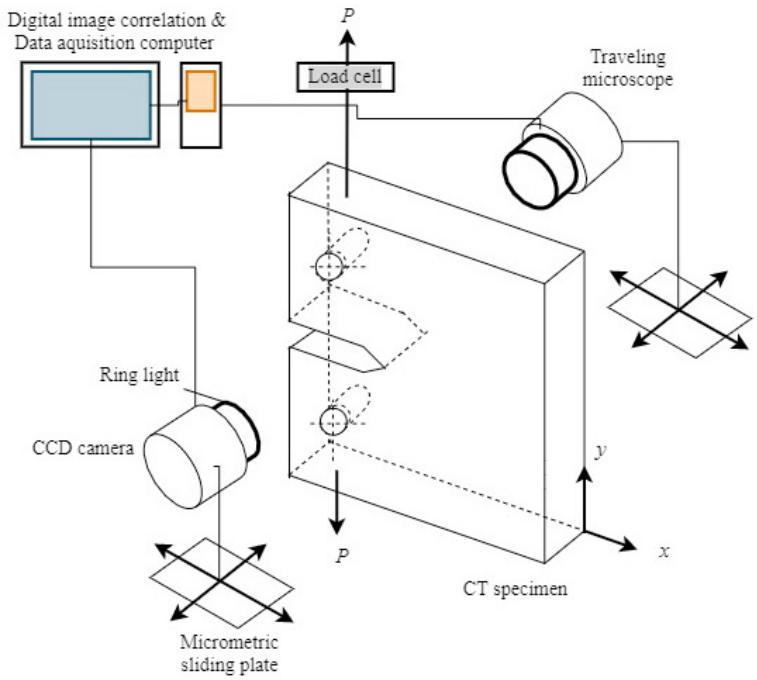

Fig.1: A schematic diagram of complete experimental setup (Yusof, Lopez-Crespo, and Withers 2013)

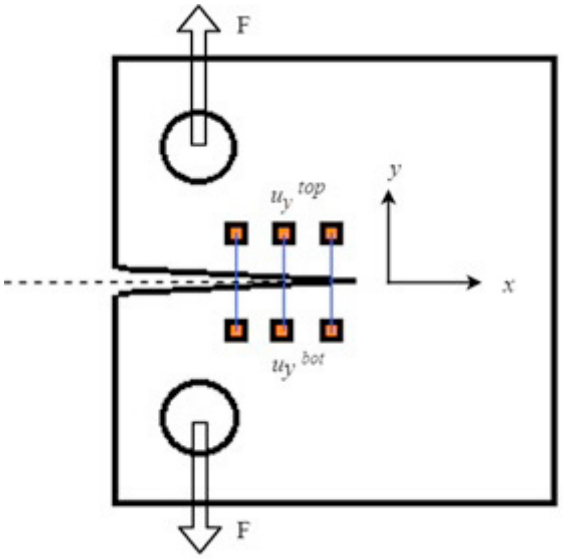

Fig.2: Schematic of CTOD measurement behind the crack-tip.

Once the location of the crack tip has been established (Lopez-Crespo et al. 2008)(López-Crespo et al. 2009) (Vasco-Olmo et al. 2017), the experimental CTOD is obtained by defining the measurement point behind the crack tip. In this case the measurement point was 104 μm behind the crack-tip. Thus, CTOD as a function of load for a complete cycle is evaluated by analyzing both the loading and unloading branches. In this way, the portion of the cycle at which the crack is closed and opened can be evaluated. In addition, from the analysis of the portion at which the crack is open, the elastic and plastic components of the CTOD can be estimated from the slope obtained from fitting of the selected data points in the CTOD versus load curves and extrapolating the linear regime to the maximum load.

4. Extraction of $CTOD_p$

The classical relation of CTOD-Load curves is not only used to study crack closure but it can be used to analyze small and large scale yielding at crack-tip, fatigue propagation under biaxial conditions (Cruces et al. 2020) and to exclude elastic deformation which is barely related to FCGR. The methodology which is being presented here is very important for efficient analysis of CTOD-Load relation utilizing the full-field displacement data from DIC (Lopez-Crespo et al. 2009)(Schreier, Orteu, and Sutton 2009). CTOD vs load curves as shown in Fig.3 can be obtained from original data where point A and E on this plot correspond to minimum and maximum loads respectively. Fig.3 shows that the major part of deformation is elastic for the current material being studied. However, only the plastic component of CTOD is responsible for fatigue crack growth, since it is linked to irreversible mechanisms. For relatively low loads, between A and B, the crack should be completely closed as shown in Fig.3 but actually there is slight slope since DIC detects very small displacements due to the sensitivity of the technique. The increase of the load opens the crack at point B. After point B, the crack opens linearly with load up to point D, which is the boundary of elastic regime. Between points D and E, there is a progressive increase of plastic deformation, which has its peak value at maximum load. The decrease of load produces reverse elastic deformation, between point E and F, with the same rate observed during loading. That's why the maximum allowable variation between the slopes of elastic deformations for loading and unloading is kept to be one percent. After point E reverse plastic deformation starts and crack closes again at point G. It is also noted that there is slight difference in opening and closing loads. This difference can be studied further and maybe considered as a very important parameter and can be linked to some phenomenon happening at crack-tip while the crack is closed.

4.1. Identification of parameters

A typical CTOD versus load curve is shown in Fig.3 in which the data points are extracted from 2D-DIC. Points B and G define crack opening and the crack closure, respectively. Points D and F define the boundaries of elastic regime during loading and unloading, respectively. Depending on the location used to measure the CTOD, a non-linear variation may occur between points B and C. Different parameters can be extracted from these characteristic points.

Crack opening level

$$U_{op} = \frac{F_B - F_{\min}}{F_{\max} - F_{\min}} \tag{4}$$

Crack closure level

$$U_{cl} = \frac{F_G - F_{\min}}{F_{\max} - F_{\min}} \tag{5}$$

It is also observed that $U_{op} \geq U_{cl}$ is always held valid for CTOD vs Load cycle.

Where F_{min} and F_{max} are the minimum and maximum load applied during the cycle, as shown in Fig.4, while F_B and F_G are the loads when crack opens during loading and closes during unloading respectively, corresponding to the points B and G shown in Fig.3.

4.2. Algorithm to obtain parameters

It is important to follow a well-defined sequence of steps for the correct extraction of parameters. The starting point is a set of points with the load and corresponding CTOD, obtained for one load cycle. The first point in Fig.4 corresponds to the minimum load, which is followed by a progressive increase of load up to its maximum value and by the subsequent return to its minimum value. The number of points is variable depending on the DIC procedures.

(i) Crack opening and closure levels

The first step is the identification of the crack opening and closure levels, i.e., the forces F_B and F_G, respectively. In Fig.5a purple data points showing the part loading curve near crack opening and green data points are part of unloading curve near crack closure, while Fig.5b is a schematic representation of the extrapolation procedure which shows the loading is applied in a finite number of increments, the crack is closed at one load step 1 and opened in the subsequent step 2. Thus, the crack is effectively opened between points 1 and 2, as highlighted in Fig.5b. The two points immediately after opening (2 and 3) are used to define a linear extrapolation to obtain the opening load. When there are plain strain conditions and crack is open from the beginning, this kind of extrapolation is not required.

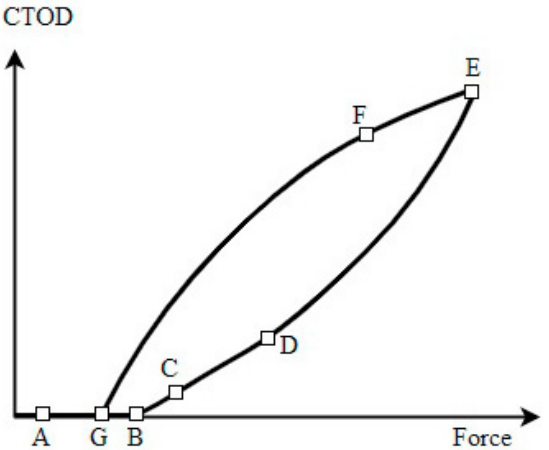

Fig.3: Schematic representation of CTOD versus load curve, including the identification of characteristic points (Marques et al. 2020).

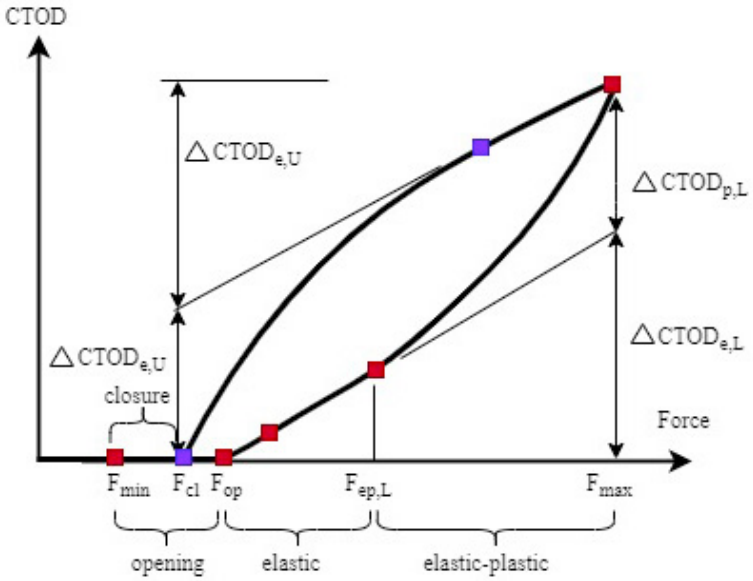

Fig.4: Parameters for fatigue crack growth analysis (Marques et al. 2020).

The crack opening load is sometimes not very clear as the data is not very smooth. This could be due to the noise in the signal from CCD camera, illumination setup, speckled surface and surface warping during experiment. To handle this issue, it is proposed that if the four consecutive values of CTOD are increasing just after zero, then the first of the four can be considered as point 2 in Figure 5b.

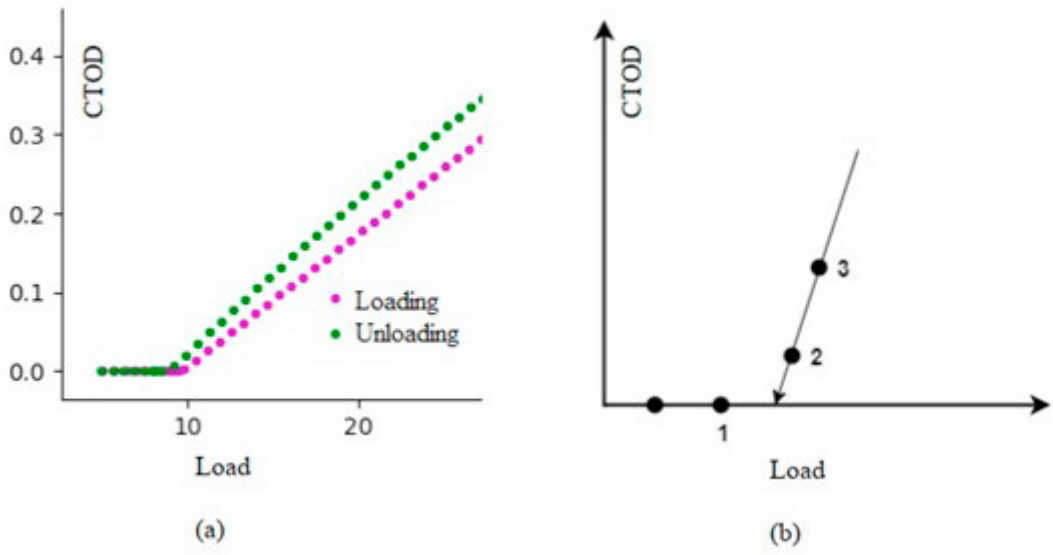

Figure 5: (a) Data points near crack opening and closure. Only some part of loading and unloading curves are shown(b) Schematic representation of the extrapolation procedure to define crack opening and closure loads (Marques et al. 2020).

(ii) Slope of the elastic regime during unloading (S_{eU})

The second step is the determination of the slope of the elastic regime. The identification is made during unloading (region EF in Fig.3) because there is no interference of the phenomena like crack closure.

The starting point corresponds to the maximum load. The number of points considered to define the slope of the elastic regime is defined using the maximization of the correlation coefficient technique. This technique involves the calculation of the least squares correlation coefficient for the first two pairs of points starting from the origin (i.e., from the maximum load). Then, the next data pair is added and the correlation coefficient is computed again. The procedure is repeated for the whole data set (unloading). The last point used to define the slope of the linear regime is dictated by the maximum correlation coefficient.

Although there are different techniques for the maximization of correlation, the one which is applied in this analysis is a built-in routine (Rolling Regression) from Python libraries as shown in Fig.6.

(iii) Elastic and plastic CTOD ranges during unloading

The elastic CTOD can now be calculated:

$$CTOD_e = S_{eU} \times F_U \tag{6}$$

where S_{eU}, is the slope of the elastic regime and F_U denotes the applied force during unloading (i.e., F_{max} -F). The maximum value of F_U is the difference between the maximum load (F_{max} =F_E) and the closure load (F_G). The plastic CTOD is the difference between the total and the elastic values:

$$CTOD_p = CTOD - CTOD_e \tag{7}$$

The plastic CTOD, $CTOD_p$ or δp, which is a main parameter for FCG analysis, is zero in the elastic regime, increasing progressively during unloading. The elastic and plastic ranges during unloading, δe and δp, respectively, are the maximum values of the elastic and plastic CTOD.

(iv) Slope of the elastic regime during loading, ($S_{e,L}$)

The next step is the determination of the slope of the elastic regime in the loading phase (region CD in Fig.3). The linear regime (CD in Fig.3) only starts after the crack is totally open. If the slope of the two points after opening is significantly different from $\delta_{e,U}$ (maximum deviation allowed usually less than 1%) the first point is rejected and the analysis moves to the next point. The procedure is repeated until the slope reaches $\delta_{e,U} \pm tol$, being tol the tolerance admitted for the slope. Therefore, the point C is the first data point after the crack opening that allows fulfilling the deviation criteria in the loading elastic regime.

(v) Elastic and plastic CTOD during loading

CTODe and CTODp components are calculated for loading using the slope calculated from the loading phase, Se,L:

$$CTOD_e = S_{e,L} \times \left(F - F_C\right) \tag{8}$$

The elastic and plastic CTOD ranges are, respectively:

$$\Delta\delta_{e,L} = S_{e,L} \times \left(F_{\max} - F\right) + \delta_C \tag{9}$$

$$\Delta\delta_{p,L} = CTOD_{\max} - \Delta\delta_{e,L} \tag{10}$$

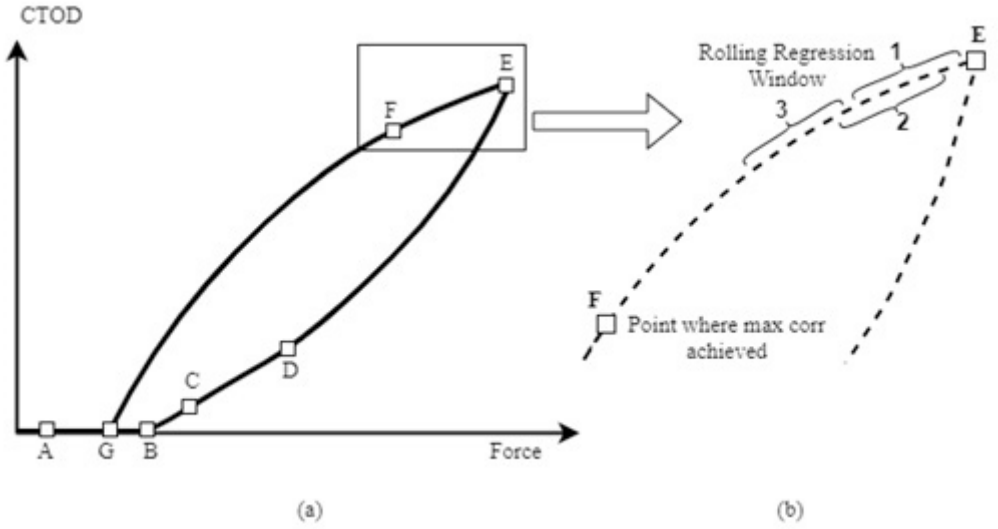

Fig.6: (a) & (b) Implementation of rolling regression to achieve maximum correlation point on the unloading curve.

5. Results and Discussion

The concept for the extraction of plastic CTOD has been utilized successfully (Vasco-Olmo et al. 2017). Total of 53 CTOD-Load data samples were collected for thick CT specimen at different stages of crack propagation. On average, five data sets for CTOD-Load (at different locations behind the crack-tip) were collected for each propagation stage. However, the data collected at 104 μm behind the crack tip was used in the current analysis. A Python program was developed using different libraries available in python language. Python matplotlib libraries were used to represent the extracted data in graphical form as shown in the Fig.7. The program automatically exports all this resultant data to excel sheets for further analysis if required. The resultant data is exported in separate columns of excel sheets as Load, CTOD, Opening load, $\Delta CTOD_{e,L}$, $\Delta CTOD_{p,L}$, $\Delta CTOD_{e,U}$ and $\Delta CTOD_{p,U}$.

As mentioned previously CTOD values against load were obtained at 104μm behind crack-tip for the current analysis. Data was collected at four different stages of crack propagation. The data for Fig.8 was collected at 25K cycles and a clear knee in Fig.8a indicating that crack remained in contact for first few loading values. Fig.8b shows the plastic component of CTOD for both loading and unloading curves. The data was collected at 45K cycles for Fig.9a showing almost similar amount of crack contact. Fig.9b shows the corresponding cyclic plastic part of CTOD. The data for Fig.10a collected at 85K showing a smaller knee indicating lesser crack contact which consequently results in larger values of $CTOD_p$ (Fig.10b). As the crack has been travelled more the data taken at 125K cycles (Fig.11a), shows small knee due to lesser amount of crack contact and increased values of $CTOD_p$ values (Fig.11b).

The calculated values of da/dN and extracted $\Delta CTOD_p$ are tabulated in Table.1. Plot of da/dN vs $\Delta CTOD_p$ (Fig.12) represents the main objective of this paper. During the fatigue process as the crack progresses, higher values of FCGR and plastic deformation are expected. This is clearly indicated from the linear relation between da/dN and $\Delta CTOD_p$.

The crack closure is found to be the major phenomena affecting load range, and consequently the plastic component of CTOD. The slope of this linear relation between da/dN and $\Delta CTOD_p$ can be regarded as material property and the difference in this slope maybe dependent on the procedure adopted or the geometry of the specimen. The present work also expresses the strength of DIC technique to be used at submicron level with good spatial resolution.

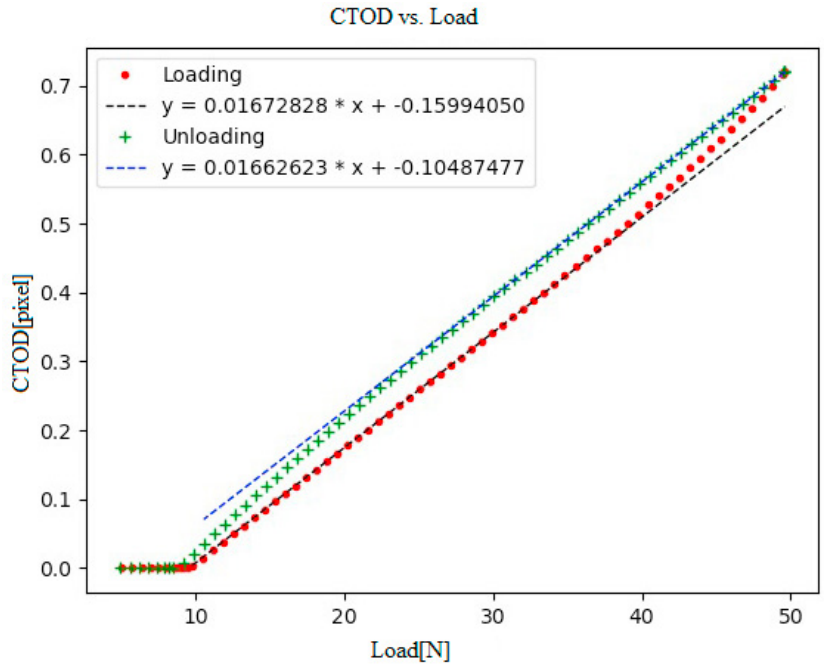

(a)

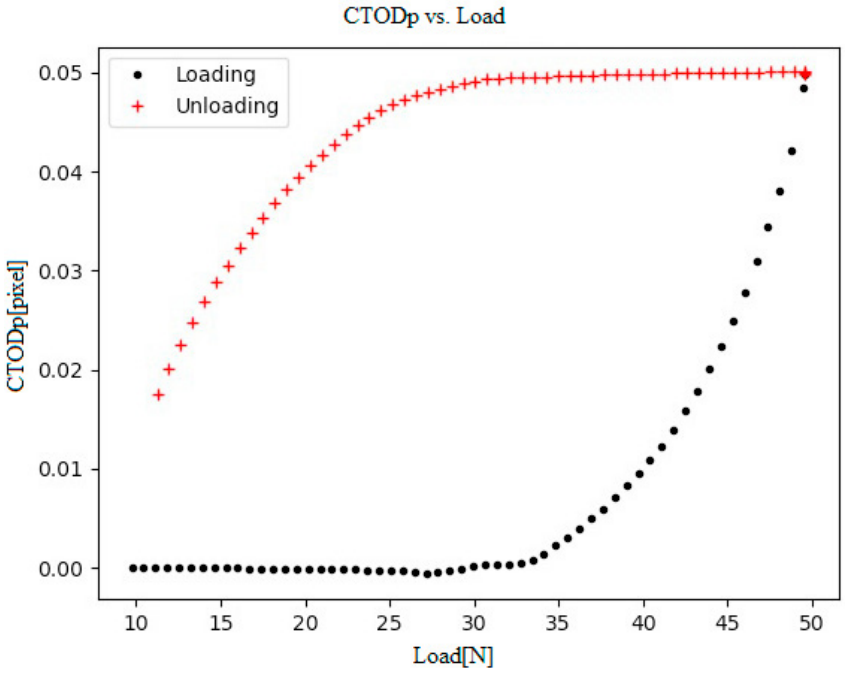

(b)

Fig.7: (a) Loading and unloading curves of CTOD vs Load. (b) CTODp vs Load.

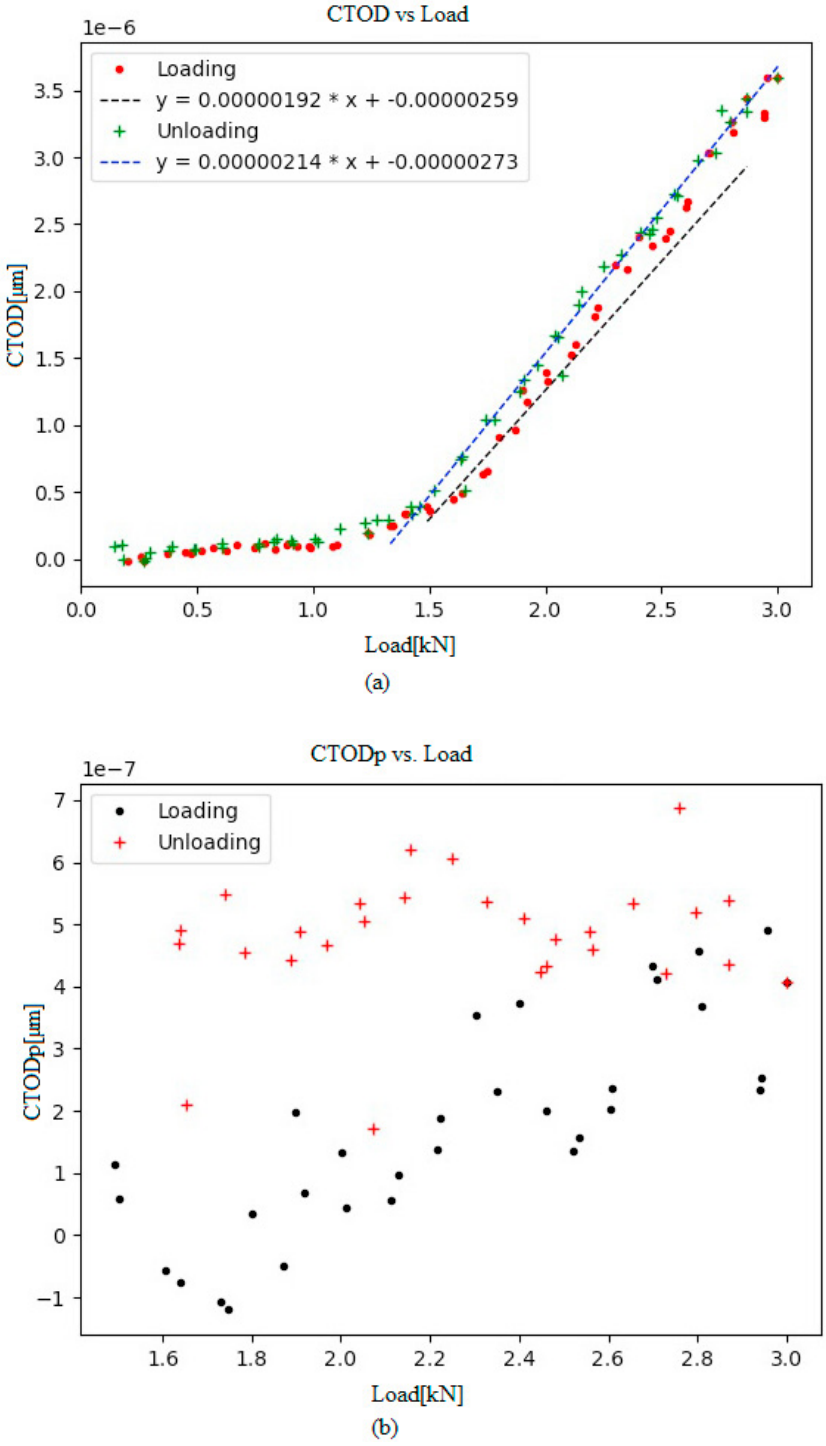

Fig.8: (a) Linear fitting of data points during loading and unloading having maximum correlation coefficient CTOD-Load after 25K cycles. (b) CTODp from the data in (a).

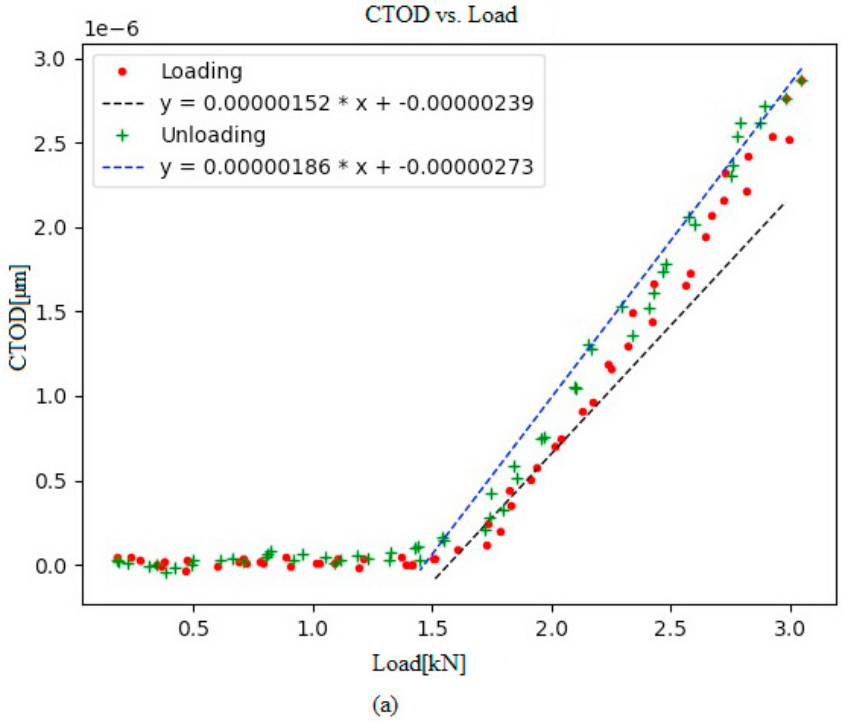

Fig.9: (a) Linear fitting of data points during loading and unloading having maximum correlation coefficient CTOD-Load after 45K cycles. (b) CTODp from the data in (a).

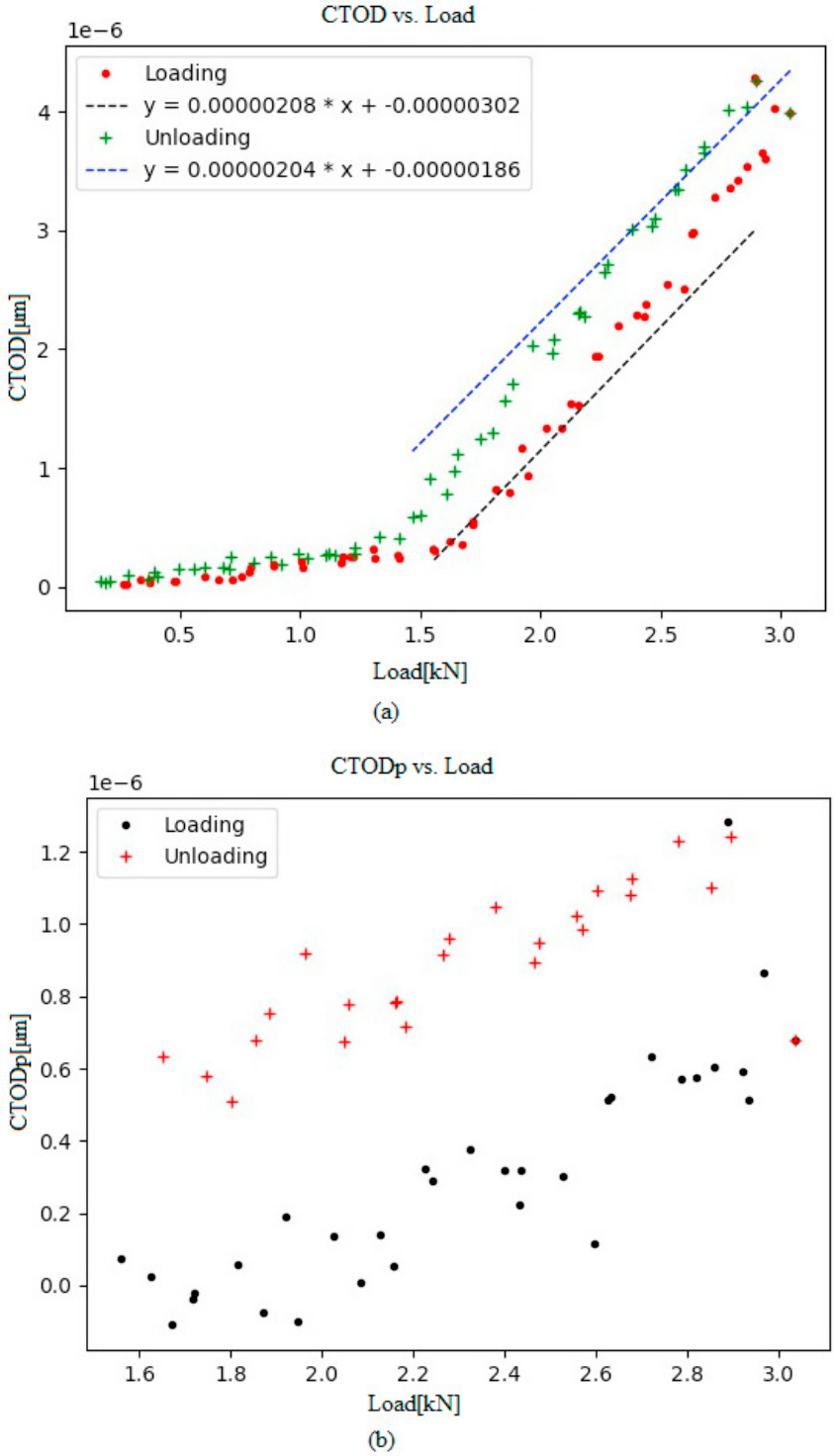

Fig.10: (a) Linear fitting of data points during loading and unloading having maximum correlation coefficient CTOD-Load after 85K cycles. (b) CTODp from the data in (a).

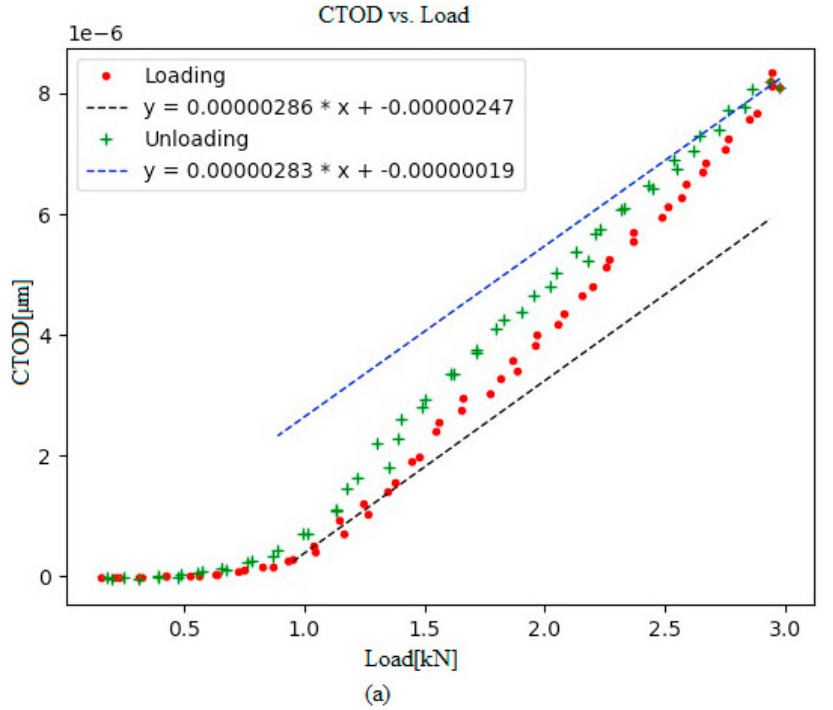

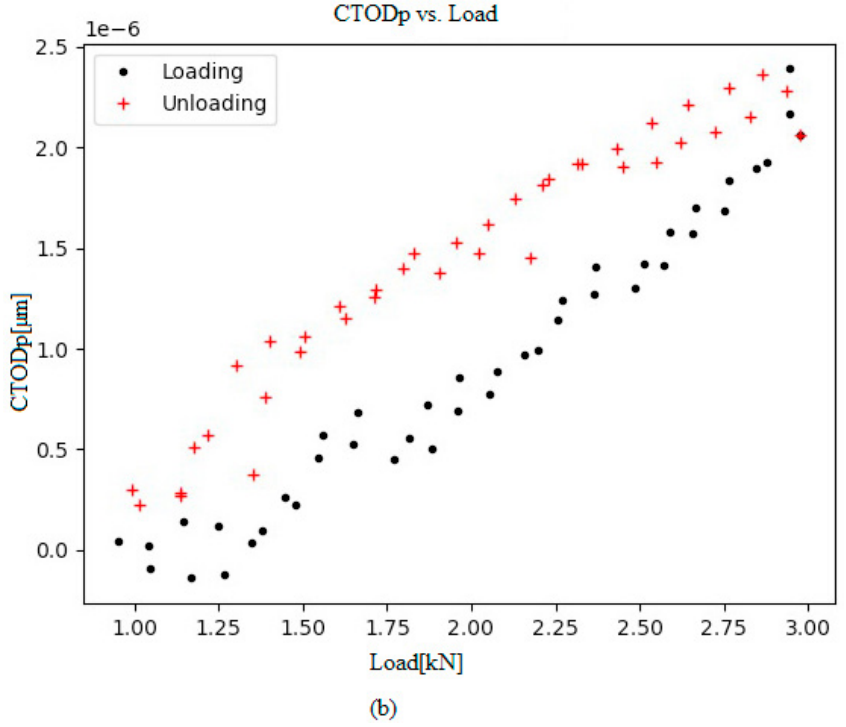

Fig.11: (a) Linear fitting of data points during loading and unloading having maximum correlation coefficient CTOD-Load after 125K cycles. (b) CTODp from the data in (a).

Table.1: ΔCTODp and da/dN values calculated at different stages of the crack propagation

Measurement Stages	N(accumulated) cycles	ΔCTODp (μm)	da/dN (μm/cycle)
1	25006	8.06564×10^{-07}	1.28577×10^{-08}
2	45000	9.84161×10^{-07}	1.34326×10^{-08}
3	85052	1.39211×10^{-06}	1.42913×10^{-08}
4	125487	2.53057×10^{-06}	1.63225×10^{-08}

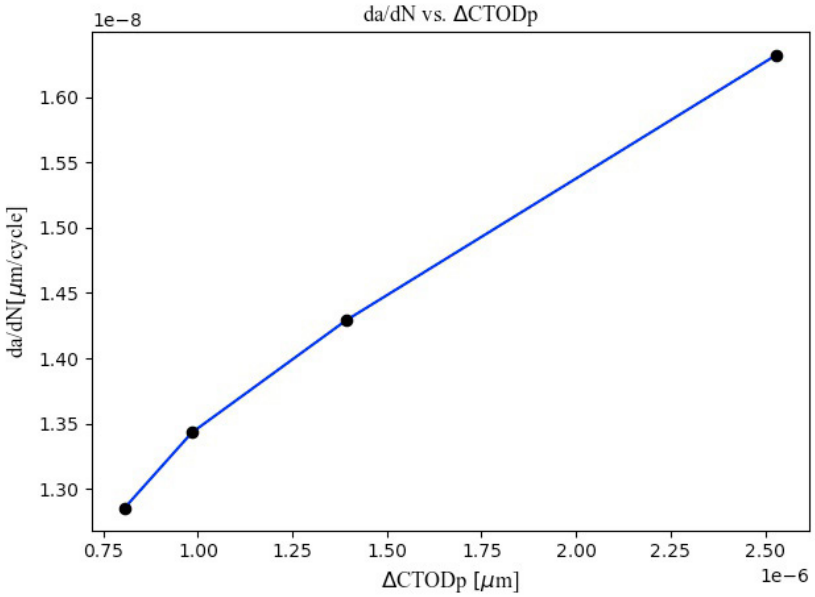

Fig.12: Plot of da/dN vs ΔCTODp for the data in Table.1.

6. Conclusion

An experimental tool for the extraction of characteristic points and parameters from CTOD vs. load data has been developed. Some interesting parameters namely, the crack opening and closure levels, the elastic and plastic ranges (ΔCTODe and ΔCTODp) for both loading and unloading curves have been drawn out.

The da/dN-$\Delta CTOD_p$ relation can used to predict fatigue crack propagation as long as the basic assumption that the plastic deformation at the crack tip is quantified by $\Delta CTOD_p$, remains valid. Fig.12 shows that the range of plastic CTOD has direct relation with FCGR. Certainly there are advantages of using this parameter over ΔK; (1) its relationship with da/dN is linear contrary to logarithmic relation between da/dN-ΔK; (2) the units of both da/dN and $\Delta CTOD_p$ are same making the slope of this relation dimensionless; (3) This slope can be regarded as material property being independent of stress ratio. Fatigue threshold is naturally included as the elastic component of CTOD is separated from this parameter.

References

Antunes, F. V. et al. 2019. Fatigue Crack Growth versus Plastic CTOD in the 304L Stainless Steel. Engineering Fracture Mechanics 214: 487–503.

Antunes, F. V., R. Branco, P. A. Prates, and L. Borrego. 2017a. Fatigue Crack Growth Modelling Based on CTOD for the 7050-T6 Alloy. Fatigue and Fracture of Engineering Materials and Structures 40(8): 1309–20.

Antunes, F. V., R. Branco, P. A. Prates, and L. Borrego. 2017b. "Fatigue Crack Growth Modelling Based on CTOD for the 7050-T6 Alloy." Fatigue and Fracture of Engineering Materials and Structures 40(8): 1309–20.

Antunes, F. V., S. M. Rodrigues, R. Branco, and D. Camas. 2016. A Numerical Analysis of CTOD in Constant Amplitude Fatigue Crack Growth. Theoretical and Applied Fracture Mechanics 85: 45–55.

Antunes, F. V., S. Serrano, R. Branco, and P. Prates. 2018. Fatigue Crack Growth in the 2050-T8 Aluminium Alloy. International Journal of Fatigue 115: 79–88.

ASTM E647−13. 2014. Standard Test Method for Measurement of Fatigue Crack Growth Rates. American Society for Testing and Materials.

Borges, M. F. et al. 2020. Effect of Kinematic Hardening Parameters on Fatigue Crack Growth. Theoretical and Applied Fracture Mechanics 106: 102501.

Chernyatin, A. S., P. Lopez-Crespo, B. Moreno, and Yu G. Matvienko. 2018. Multi-Approach Study of Crack-Tip Mechanics on Aluminium 2024 Alloy. Theoretical and Applied Fracture Mechanics 98: 38–47.

Christopher, C. J., M. N. James, E. A. Patterson, and K. F. Tee. 2007. Towards a New Model of Crack Tip Stress Fields. International Journal of Fracture 148(8): 361.

Cruces, A. S. et al. 2020. Study of the Biaxial Fatigue Behaviour and Overloads on S355 Low Carbon Steel. International Journal of Fatigue 134: 105466.

Donald, Keith, and Paul C. Paris. 1999. An Evaluation of ΔKeff Estimation Procedures on 6061-T6 and 2024-T3 Aluminum Alloys. International Journal of Fatigue 21: S47–57.

Elber, W. 1971. The Significance of Fatigue Crack Closure. ASTM Special Technical Publication: 230–42.

Ewalds, H L, and R J H Wanhill. 1984. Fracture Mechanics. London: Edward Arnold.

GmbH, La Vision. 1999. PIV Software Manual. https://www.lavision.de/de/downloads/manuals/systems.php.

Ktari, A. et al. 2014. A Crack Propagation Criterion Based on ΔCTOD Measured with 2D-Digital Image Correlation Technique. Fatigue and Fracture of Engineering Materials and Structures 37(6): 682–94.

Kujawski, Daniel. 2001a. A New (ΔK+Kmax)0.5 Driving Force Parameter for Crack Growth in Aluminum Alloys. International Journal of Fatigue 23(8): 733–40.

Kujawski, Daniel. 2001b. Enhanced Model of Partial Crack Closure for Correlation of R-Ratio Effects in Aluminum Alloys. International Journal of Fatigue 23(2): 95–102.

Larsson, S. G., and A. J. Carlsson. 1973. Influence of Non-Singular Stress Terms and Specimen Geometry on Small-Scale Yielding at Crack Tips in Elastic-Plastic Materials. Journal of the Mechanics and Physics of Solids 21(4): 263–77.

Lopez-Crespo, P. et al. 2008. The Stress Intensity of Mixed Mode Cracks Determined by Digital Image Correlation. Journal of Strain Analysis for Engineering Design 43(8): 769–80.

Lopez-Crespo, P. et al. 2009. Some Experimental Observations on Crack Closure and Crack-Tip Plasticity. Fatigue and Fracture of Engineering Materials and Structures 32(5): 418–29.

Lopez-Crespo, P. et al. 2013. Overload Effects on Fatigue Crack-Tip Fields under Plane Stress Conditions: Surface and Bulk Analysis. Fatigue and Fracture of Engineering Materials and Structures 36(1): 75–84.

López-Crespo, P. et al. 2009. Study of a Crack at a Fastener Hole by Digital Image Correlation. Experimental Mechanics 49: 551–59.

Lopez-Crespo, P., D. Camas, F. V. Antunes, and J. R. Yates. 2018. A Study of the Evolution of Crack Tip Plasticity along a Crack Front. Theoretical and Applied Fracture Mechanics 98: 59–66.

Lugo, M., and S. R. Daniewicz. 2011. The Influence of T-Stress on Plasticity Induced Crack Closure under Plane Strain Conditions. International Journal of Fatigue 33(2): 176–85.

Marques, Bruno et al. 2020. Numerical Tool for the Analysis of CTOD Curves Obtained by DIC or FEM. Fatigue and Fracture of Engineering Materials and Structures 43(12): 2984–97.

Miarka, Petr et al. 2020a. Evaluation of the SIF and T-Stress Values of the Brazilian Disc with a Central Notch by Hybrid Method. International Journal of Fatigue 135(February): 105562.

Miarka, Petr et al. 2020b. Influence of the Constraint Effect on the Fatigue Crack Growth Rate in S355 J2 Steel Using Digital Image Correlation. Fatigue and Fracture of Engineering Materials and Structures 43(8): 1703–18.

Noroozi, A. H., G. Glinka, and S. Lambert. 2005. A Two Parameter Driving Force for Fatigue Crack Growth Analysis. International Journal of Fatigue 27(10–12): 1277–96.

Paris, P., and F. Erdogan. 1963. A Critical Analysis of Crack Propagation Laws. Journal of Fluids Engineering, Transactions of the ASME: 528–33.

Rice, J. R. 1967. Mechanics of Crack Tip Deformation and Extension by Fatigue. Fatigue Crack Propagation, ASTM STP 415, Am. Soc. Testing Mats.

Schreier, Hubert, Jean José Orteu, and Michael A. Sutton. 2009. Image Correlation for Shape, Motion and Deformation Measurements: Basic

Concepts,Theory and Applications Image Correlation for Shape, Motion and Deformation Measurements: Basic Concepts, Theory and Applications.

Vasco-Olmo, J. M., F. A. Díaz, F. V. Antunes, and M. N. James. 2017. Experimental Evaluation of CTOD in Constant Amplitude Fatigue Crack Growth from Crack Tip Displacement Fields. Frattura ed Integrita Strutturale 11(41): 157–65.

Vasudevan, A. K., K. Sadananda, and N. Louat. 1992. Reconsideration of Fatigue Crack Closure. Scripta Metallurgica et Materiala 27(11): 1673–78.

Yusof, F., P. Lopez-Crespo, and P. J. Withers. 2013. Effect of Overload on Crack Closure in Thick and Thin Specimens via Digital Image Correlation. International Journal of Fatigue 56: 17–24.

Yusof, F., and P. J. Withers. 2009. Real-Time Acquisition of Fatigue Crack Images for Monitoring Crack-Tip Stress Intensity Variations within Fatigue Cycles. Journal of Strain Analysis for Engineering Design 44(2): 149–58.

Zheng, X. et al. 2013. Numerical Modeling of Fatigue Crack Propagation Based on the Theory of Critical Distances. Engineering Fracture Mechanics 114: 151–65.